JOURNAL OF COMPUTATIONAL PHYSICS 73, 233–243 (1987)

Redesign of a Supercritical Wing in the Presence of an Engine Nacelle

DAVID S. ROSS

Courant Institute of Mathematical Sciences, New York, New York 10012

Received January 15, 1986; revised June 17, 1986

A method for modelling an engine nacelle in a compressible flow using a source distribution is described. The incorporation of this technique into a free boundary supercritical wing design code is discussed. Results of calculations made with this code are presented. A method for calculating wave drag is also described. © 1987 Academic Press, Inc.

1. INTRODUCTION

A principal goal of computational transonic aerodynamics is to develop computational methods for the analysis of transonic flows and for the design of efficient transonic aircraft. We are interested, in particular, in the problem of designing wings with only weak shocks at a given Mach number and angle of attack. Methods exist for the design of shockless transonic airfoils [1, 3] and for computing the transonic flow about a given wing [8, 9]. One approach to the design of a low drag transonic swept wing is to start with a shockless airfoil in each wing section. Three-dimensional effects will cause shocks on such a wing, but we expect them not to be too severe. By small readjustments of the wing surface, which can be made by a code which treats the wing surface as a free boundary, we can redesign the wing to reduce the strength of the shocks. Our method takes this program one step further. If an obstacle, such as an engine nacelle, is placed in the flow near an almost shockless wing, sizeable shocks can be expected to appear on the wing. We have incorporated a model of such an obstacle into the free boundary design code FL22INV in order to redesign wings under more realistic conditions.

Our work is an extension of that of Bauer *et al.* [4]. Their method is based on the Murman–Cole relaxation procedure. The idea is to specify a reasonable, smooth pressure distribution over the upper wing surface and to treat that surface as a free boundary. The free boundary moves during the course of the relaxation procedure so that the prescribed pressure distribution is achieved. We have incorporated in their code a model of an engine nacelle by adding an inhomogeneous term to the potential equation. The obstacle is thus represented by a fluid source, as in the method of images of incompressible flow theory.

The basic difficulty in computing the flow about a wing and nacelle combination is the generation of an appropriate computational grid. If we were interested in the

0021-9991/87 $3.00

details of the flow about a nacelle, this difficulty would be unavoidable. However, our goal is only to model the effect of a nacelle on the flow about a wing. Specifically, we want to be able to redesign a wing to eliminate the wave drag associated with the shocks on the wing caused by the presence of a nacelle. For this purpose our crude model of a nacelle, which allows us to avoid the grid generation problem, is sufficient.

2. Computational Procedure

We consider the irrotational, isentropic flow of air past a swept wing on a wall, with a mass source distribution f. Such a flow is governed by the inhomogeneous potential equation

$$(c^2-u^2)\,\phi_{xx}+(c^2-v^2)\,\phi_{yy}+(c^2-w^2)\,\phi_{zz}-2uv\phi_{xy}-2uw\phi_{xz}-2vw\phi_{yz}=\frac{c^2}{\rho}f \qquad (1)$$

for the velocity potential ϕ, which is related to the velocity components by $\nabla\phi=(u, v, w)$. We normalize ϕ so $|\nabla\phi|=1$ in the free stream. To enforce this free stream condition we write $\phi=x\cos(\alpha)+y\sin(\alpha)+G$, where α is the angle of attack. We impose the decay condition $\partial G/\partial n+\xi G=0$ on G at a control surface [4]. The constant ξ is fixed empirically. The density ρ, the pressure $P=\rho^{1.4}$, and the square of the sound speed $c^2=\partial P/\partial\rho$, can all be expressed in terms of ϕ via Bernoulli's law,

$$0.5\,|\nabla\phi|^2+2.5c^2=0.5+\frac{2.5}{M_\infty^2},$$

where M_∞ is the free stream Mach number. The normal derivative of ϕ is zero on the wing surface and on the wall. A linearized model of the vortex sheet is used [9]. At a shock in this isentropic flow model, mass and the tangential momentum components are conserved, but the normal momentum component must have a jump since entropy is conserved.

For the computation, the physical space is mapped to a computational domain where a rectangular finite difference grid is set up. First a square root transformation is used to map the physical space to half-space. This mapping takes the wing surface to a surface $Y=S(X, Z)$ in parabolic coordinates. Next a shearing transformation $\bar{Y}=Y-S(X, Z)$, $\bar{X}=X$, $\bar{Z}=Z$, takes the wing to a patch on the plane $\bar{Y}=0$. A final mapping takes the $\bar{X}$, $\bar{Y}$, $\bar{Z}$ quadrant containing the flow domain into a box. We also use this mapping to concentrate grid points near the source, i.e., near the points where $f\neq 0$. The purpose of this grid squeezing, which is accomplished with polynomials, is discussed in the next section. We choose $X_{\max}$ and $Z_{\max}$ so that the image of the wing lies in the rectangle $0\leqslant\bar{Z}<Z_{\max}$, $|\bar{X}|<X_{\max}$ in the plane $\bar{Y}=0$. We choose $\tilde{Y}_a$, $\tilde{Y}_b$, $\tilde{Z}_a$, $\tilde{Z}_b$ with $\tilde{Y}_a\leqslant\tilde{Y}_b$ and $\tilde{Z}_a\leqslant\tilde{Z}_b$ such that the source representing the nacelle lies on the line $\bar{Y}=\frac{1}{2}(\tilde{Y}_a+\tilde{Y}_b)$,

$\tilde{Z} = \frac{1}{2}(\tilde{Z}_a + \tilde{Z}_b)$ in the computational domain. We can write explicit formulas only for the inverse mapping

$$\bar{X} = \begin{cases} \tilde{X}, & |\tilde{X}| < X_{\max} \\ \pm X_{\max} + \dfrac{\tilde{X} - \pm X_{\max}}{\left(1 - \left(\dfrac{\tilde{X} - \pm X_{\max}}{1 - X_{\max}}\right)^2\right)^{1/2}}, & \pm\tilde{X} > X_{\max} \end{cases}$$

$$\bar{Y} = \begin{cases} \dfrac{1}{2}\dfrac{\tilde{Y}}{(1-\tilde{Y}^2)^{1/2}}, & 0 \leqslant \tilde{Y} \leqslant \tilde{Y}_a,\ \tilde{Y}_b \leqslant \tilde{Y} \\ \dfrac{1}{2}\dfrac{\tilde{Y}}{(1-\tilde{Y}^2)^{1/2}} + P_y(\tilde{Y}), & \tilde{Y}_a < \tilde{Y} < \tilde{Y}_b \end{cases}$$

$$\bar{Z} = \begin{cases} \tilde{Z}, & 0 \leqslant \tilde{Z} \leqslant \tilde{Z}_a,\ \tilde{Z}_b \leqslant \tilde{Z} \leqslant Z_{\max} \\ \tilde{Z} + P_z(\tilde{Z}), & \tilde{Z}_a \leqslant \tilde{Z} \leqslant \tilde{Z}_b \\ Z_{\max} + \dfrac{\tilde{Z} - Z_{\max}}{\left(1 - \left(\dfrac{\tilde{Z} - Z_{\max}}{1 - Z_{\max}}\right)^2\right)^{1/2}}, & Z_{\max} \leqslant \tilde{Z}. \end{cases}$$

Here P_y and P_z are seventh-degree polynomials which are constructed so that the mappings are twice continuously differentiable. This leaves two parameters for each polynomial. These are used to specify the values of the polynomials and their derivatives at the midpoints of the intervals. The values of the derivatives determine the concentration of grid points near the source.

The difference equations, which are based on Jameson's rotated scheme [8], are solved by line relaxation. We use a nonconservative scheme in order to model the interaction of the boundary layer and the shocks [6].

For a design run, a smooth upper surface speed distribution is specified. An exponential spline routine makes it possible to construct such a distribution from a few parameters based on the wing's original speed distribution [7, 10]. The upper wing surface is treated as a free boundary which is allowed to move during the course of the relaxation procedure in order to achieve the specified speed distribution. If the relaxation iterations are viewed as steps in an artificial time parameter t, the rule for the motion of the wing surface can be written [7]

$$a_1 S_{xt} + a_2 S_t = Q + a_3 Q_{S_x} Q_x + a_4 Q_{S_z} Q_z,$$

where $Q = q(X, Z) - q_0(X, Z)$ is the difference between the computed and the specified speed distributions. This rule, which is based on linearized theory [5], is applied subject to a constraint $S \geqslant S_0$, where S_0 represents an inner wing structure. The constants a_j are adjusted so that the iterations converge.

We generally terminate the computation once the speed distribution is smoothed out, which is usually long before the design procedure converges.

3. Model of an Engine Nacelle

In the incompressible case, source distributions for modeling obstacles are often made up of delta functions or point sources. In the corresponding compressible case we solve a discretized version of the inhomogeneous potential equation (1) with a source distribution given by a function $f_{i,j,k}$ which is nonzero at only one or two grid points. It is important to keep in mind that a mass source distribution f yields an inhomogeneous term $(c^2/\rho)f$ for the potential equation.

With such a source distribution, we have limited control over the shape of the obstacle. It will be a semi-infinite cylinder. If the grid size near the source is adjusted correctly, as we shall discuss below, the cylinder will be circular and will have approximately the shape of a Rankine ogive. Fortunately, such a shape is sufficiently close to the shape of an engine nacelle for our purpose.

For simplicity assume that f is nonzero at exactly one grid point (x_0, y_0, z_0), with indices i_0, j_0, k_0. If the asymptotic corss-sectional area of the nacelle A_∞ is specified, we can determine the value of f_0 which will produce this area by integrating the mass equation, $\nabla \cdot (\rho \nabla \phi) = f$. In order to perform the integration we must extend f to a function of the continuous variables. We do this by the formula

$$f(\tilde{X}, \tilde{Y}, \tilde{Z}) = f_0 \left(1 - \left(\frac{\tilde{X} - \tilde{X}_0}{\Delta x}\right)^2\right)\left(1 - \left(\frac{\tilde{Y} - \tilde{Y}_0}{\Delta y}\right)^2\right)\left(1 - \left(\frac{\tilde{Z} - \tilde{Z}_0}{\Delta z}\right)^2\right)$$

in the computational domain for points in grid boxes adjacent to the source point, and elsewhere we set $f = 0$. Of several integration schemes which were tried this one gave the best results; i.e., this one best represents the way the difference scheme responds to the source. The integration yields

$$\rho_\infty A_\infty = \iiint f \, dx \, dy \, dz = \frac{8}{27} f_0 V,$$

where V is the total volume in physical space of the grid boxes adjacent to the source.

For fixed A_∞ we have a one-parameter family of values of f and V. For large V the obstacle will not be clearly defined; i.e., there will be no stagnation point, no dividing streamline, and no way of establishing a shape and position for the obstacle. This situation can be illustrated by the following example of a two-dimensional incompressible flow. We introduce a radially symmetric source distribution given by a Gaussian $(k/\beta)\, e^{-r2/\beta}$ into a uniform flow with potential x. The constant k is proportional to the source strength. The parameter β measures the concentration of the source, with small beta representing high concentration. The velocity on the x axis is then given by

$$u(x, 0) = 1 + \frac{k}{x}(1 - e^{-x^2/\beta}).$$

In the limit as $\beta \to 0$ we get the point source solution. An application of the mean value theorem to the function $xu(x, 0)$ shows that no stagnation point and thus no dividing streamline exists for $\beta \geq 2k^2$.

In the numerical solution of the potential equation a similar situation exists, with the grid size taking the place of β. In order to represent a nacelle on the coarse grids which must often be used for three-dimensional calculations, we must reduce the grid size near the source. This local grid refinement is also necessary in some cases to obtain an obstacle with an asymptotically circular cross section; if the grid size in one direction is substantially larger than that in another, we will obtain an oblong cross section. We adjust the grid spacing by altering the mapping to computational coordinates, using the polynomials $P_y(\tilde{Y})$ and $P_z(\tilde{Z})$ [10].

At transonic speeds cavitation may occur near a source which is sufficiently strong and concentrated to produce a clearly defined obstacle of the size of an engine nacelle. We overcome this difficulty by replacing the potential equation (1) with a constant coefficient equation near the source. The equation we use is obtained by replacing the velocity components u, v, and w, and the sound speed c by u_∞, v_∞, w_∞, and $1/M_\infty$, i.e., by freezing the coefficients at their free stream values. This amounts to treating the fluid as incompressible near the source. In physical coordinates the corresponding equation becomes

$$\rho_\infty \left(\left(\frac{1}{M_\infty^2} - \cos^2 \alpha \right) \phi_{xx} + \left(\frac{1}{M_\infty^2} - \sin^2 \alpha \right) \phi_{yy} \right.$$
$$\left. - 2 \cos \alpha \sin \alpha \phi_{xy} + \left(\frac{1}{M_\infty^2} \right) \phi_{zz} \right) = \frac{1}{M_\infty} f, \tag{2}$$

where α is the angle of attack.

The use of this equation near the source in no way affects the validity of our solution; the altered equation is applied only inside the nacelle. We are not concerned with the details of the flow in this region, but only with producing an obstacle. The use of Eq. (2) near the source also facilitates the specification of the nacelle size. In our formulation, in which we specify the inhomogeneous term for the potential equation, the effective source strength in the compressible case is a function of the density at the source point. At the surface where the fluid flows out of the constant coefficient region, ρ_∞ is a good approximation to the density. Therefore we can accurately estimate the nacelle size by specifying the source strength as if for an incompressible flow with constant density ρ_∞.

No special considerations are necessary for differencing in the constant coefficient region. The type-sensitive scheme automatically treats the equation as elliptic, since we freeze the speed at a subsonic value.

When ϕ has been computed we locate and plot the engine nacelle by tracing streamlines near its surface. In this way we also check its asymptotic cross-sectional area. We trace the streamlines by solving the system of ordinary differential equations

$$\frac{d}{dt}(\tilde{X}, \tilde{Y}, \tilde{Z}) = JJ^T(\phi_{\tilde{X}}, \phi_{\tilde{Y}}, \phi_{\tilde{Z}})$$

in the computational domain, where J is the Jacobian matrix of the coordinate mapping. In order to carry out the integration we must interpolate the derivatives of ϕ for points not on the grid. We assume that ϕ is the restriction to grid points of a smooth function of the same name. At a point $(\tilde{X}, \tilde{Y}, \tilde{Z})$ we expand ϕ in a power series and express ϕ at neighboring grid points in terms of this series. We then take a weighted average of these expressions to obtain a second-order approximation to the desired derivative.

We first locate the stagnation point, which we take as the tip of the nacelle. Once the stagnation point has been found, we construct a small circle in a plane perpendicular to the free stream velocity, just upstream of the stagnation point. Several streamlines are begun at equal spacings on this circle. The streamlines are traced using a fourth-order, variable step-size, Adams predictor-corrector method. They are terminated in the far field on a plane perpendicular to the free stream, and a trigonometric interpolant is passed through the termination points. We use this interpolant to compute the final stream tube cross-sectional area, and then subtract off the area due to the mass flux into the stream tube through the original circle to obtain the nacelle cross-sectional area. The area computed in this way generally agrees with the input A_∞ to within 10–15 %.

The nacelle is plotted along with the wing and shocks (see Fig. 3), as a circular cylinder of area A_∞ centered on the line $x = x_0$.

4. Wave Drag

Any method for redesigning transonic wings must be based on an accurate method for approximating wave drag. In this section we present such a method due to Garabedian [6]. A basic difficulty in computing wave drag, numerically or experimentally, is separating it from other forms of drag. For a flow with sharp shocks, we can compute the wave drag from the jumps in the flow quantities at the shocks. However, flows computed by artificial viscosity methods have smeared shocks, so it is not clear how to define the shock jumps. The method we shall describe overcomes these difficulties by computing the wave drag as an integral of the artificial viscosity.

Retarded difference schemes capture shocks by effectively adding artificial viscosity to the equation in the supersonic zone. For simplicity we shall discuss difference schemes for the two-dimensional potential equation. If we expand the numerical solution in a Taylor series and drop terms of higher than first order in the grid size h, we obtain the modified equation

$$(c^2 - u^2)\phi_{xx} + (c^2 - v^2)\phi_{yy} - 2uv\phi_{xy} = \eta \tag{3}$$

in the supersonic zone. We consider only schemes which are second-order accurate in the subsonic zone, so the modified equation agrees with the potential equation there. The artificial viscosity η is $O(h)$ in regions of smooth flow. The form of η characterizes the difference scheme. For example, $\eta = h(c^2 - u^2)\,\phi_{xxx}$ for the standard nonconservative scheme on a rectangular grid, $\eta = h(c^2/\rho)(\rho\phi_x)_{xx}$ for the analogous conservative scheme. Rotated differencing and mapped coordinates, both of which are used in our code, complicate the expression for η.

To recover the mass or x-momentum equations from the potential equation we multiply by ρ/c^2 or $\rho u/c^2$. From Eq. (3) we thus see that the artificial viscosity yields a mass source $(\rho/c^2)\,\eta$ and an x-momentum source $(\rho u/c^2)\,\eta$ in the supersonic zone D. An amount

$$\iint_D \frac{\rho u}{c^2}\,\eta\,dx\,dy$$

of x-momentum is created per unit time in the supersonic zone, and an amount

$$u_x \iint_D \frac{\rho}{c^2}\,\eta\,dx\,dy$$

flows into the far field. The momentum rise is balanced by a force

$$F = \iint_D (u - u_\infty)\,\frac{\rho}{c^2}\,\eta\,dx\,dy \tag{4}$$

on the wing which, for a conservative scheme, is the wave drag.

For a nonconservative scheme the expression (4) will be of second order in the shock strength, whereas the wave drag is of third order. To obtain the correct expression for the wave drag D_W we must subtract

$$\lim_{h\to 0}(c_* - u_\infty) \iint_D \frac{\rho}{c^2}\,\eta\,dx\,dy$$

from (4) to yield

$$D_w = \lim_{h\to 0} \iint_D (u - c^2)\,\eta\,dx\,dy \tag{5}$$

where c_* is the critical speed. This expression is of third order in the shock strength, and it reduces in the limit $h \to 0$ to the standard line integral for the wave drag [10]. The correction term has the following interpretation: it is the force which decelerates the excess mass produced by the nonconservative scheme from the critical speed c_*, which is the speed it has when it leaves the supersonic zone, to the far field speed u_∞. Since this force is a numerical effect, it must not be considered part of the wave drag.

For particular forms of η, the expression (5) can be integrated by parts to yield expressions with positive integrands. For example, for the nonconservative η described above we have

$$D_w = \lim_{h \to 0} 2h \iint_D \frac{\rho}{c^2} \phi_{xx}^2 (u^2 - c^2)\, dx\, dy, \tag{6}$$

up to fourth order in the shock strength. We can use this type of expression to show that the entropy condition is enforced [10]. The integrand of such an expression provides a local measure of wave drag which is useful for wing redesign, shock plotting (cf. Figs. 1 and 2), and local grid refinement.

In practice we simply drop the limit in expression (6), and evaluate the integrand using central differences. The integral is computed by the trapezoid rule. We exclude contributions from rarefaction waves since these vanish in the limit.

5. Computational Results

In this section we discuss the results of a series of runs of our code. We started with an analysis run followed by a design run. Then another analysis run was made with a nacelle inserted in the flow. The final run was a design run with the nacelle in place. For the series described here, the nacelle was above and behind the wing.

The development of the code and some crude grid tests were done on a VAX 11/780 at the Courant Institute. The fine grid tests described here were made on the CRAY E computer of the Lawrence Livermore Laboratory using a vectorized relaxation routine which was written by F. Bauer. Analysis runs took, on the average, 7 or 8 min of CPU time on the CRAY, and design runs took about 10, using a $192 \times 28 \times 24$ grid.

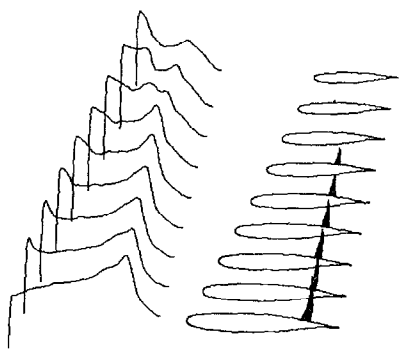

Fig. 1. Original wing.

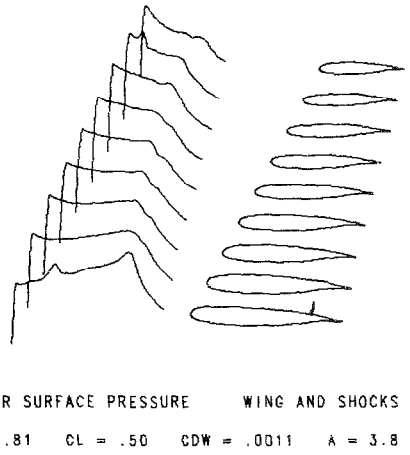

FIG. 2. Redesigned wing.

The wing we used was based on a supercritical airfoil designed by J. Sanz with a complex characteristic hodograph code [3]. The airfoil was designed to be shockless at $M_\infty = 0.75$ and $C_L = 0.5$. The thickness-chord ratio is 0.13. The leading edge was swept back 30° and the wing was tapered linearly so the chord at the wing tip was 0.56 of the chord at the root. The aspect ratio was 3.8.

Some corrections to the original wing specificatons were made to account for three-dimensional effects. In order to obtain an effective free stream Mach number of 0.75 normal to the wing we divided 0.75 by the cosine of the mean sweep angle so $M_\infty = 0.81 = 0.75/\cos(22°)$. Following this reasoning we note that the thickness-chord ratio by the same factor, so we also thinned the wing by a factor of $\cos(22°)$. The wing was twisted up 2.4° at the root relative to the tip.

Figure 1 shows the plotted output from the initial analysis run. A wave drag coefficient $C_{DW} = 0.0060$ is associated witht the strong shock wave which terminates the supersonic zone. In Fig. 2 we see the wing after it has been redesigned using the free boundary feature of the code. The wave drag is down to $C_{DW} = 0.0011$. A weak shock remains near the wing root. This is typical of our experience with the design code.

Figure 3 shows the results of an analysis run with a nacelle above and behing the redesigned wing. The nacelle diameter is 0.25 of the chord in the span station of the nacelle. A wave drag coefficient $C_{DW} = 0.0028$ is associated with the shock which has reappeared at the rear of the supersonic zone. The shock is, on the average, 10 % forward of its position on the original wing. In the span station of the nacelle it has moved forward by 16 %. The angle of attack was increased from 0.7° to 2.0° to compensate for the loss of lift due to the presence of the nacelle. This has caused the shock near the wing tip, which is barely noticeable in Fig. 1, to increase in strength. The loss of lift is not distributed uniformly along the span; there is a marked dip in the lift in the span station containing the nacelle. In order to recover

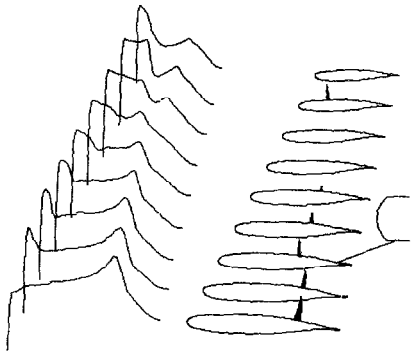

FIG. 3. The wing from Fig. 2 with a nacelle.

the original lift distribution it was necessary to twist the wing sections near the nacelle.

Results from the final run are shown in Fig. 4. Here the wing has been redesigned with the nacelle in place. The wing section in the span station of the nacelle has been twisted an additional 0.5° in order to recover the original lift distribution. The wave drag is down to $C_{DW}=0.0007$. The shocks are essentially gone even at the wing root where a shock persisted after our first design run.

Other tests of the code were made with the nacelle in various positions. In all cases we were able to eliminate the shocks by first twisting the wing locally to restore the lift distribution and then applying the free boundary iteration.

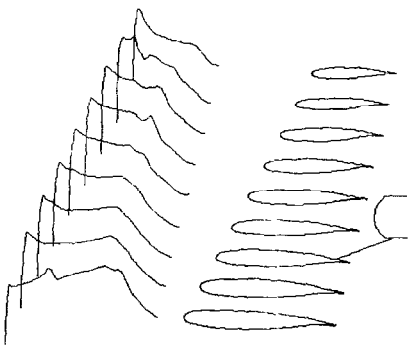

FIG. 4. Wing after being redesigned with the nacelle in place.

ACKNOWLEDGMENTS

I thank Professor P. R. Garabedian, who suggested this problem, and Dr. F. Bauer, for their advice and support. This work was supported by the Applied Mathematical Sciences subprogram of the Office of Energy Research, U.S. Department of Energy under Contract DE-AC02-76ERO3077; National Science Foundation Grant DMS-8320430; and NASA-Ames Research Center Grant NAG2-345.

REFERENCES

1. F. BAUER, P. GARABEDIAN, AND D. KORN, *A Theory of Supercritical Wing Sections with Computer Programs and Examples*, Lecture Notes in Economics and Mathematical Systems Vol. 66 (Springer-Verlag, New York, 1972).
2. F. BAUER, P. GARABEDIAN, A. JAMESON, AND D. KORN, *Supercritical Wing Sections II, a Handbook*, Lecture Notes in Economics and Mathematical Systems Vol. 108 (Springer-Verlag, New York, 1975).
3. F. BAUER, P. GARABEDIAN, AND D. KORN, *Supercritical Wing Sections III*, Lecture Notes in Economics and Mathematical Systems Vol. 150 (Springer-Verlag, New York, 1977).
4. F. BAUER, P. GARABEDIAN, AND G. MCFADDEN, "The NYU Inverse Swept Wing Code," NASA CR3662, 1983 (unpublished).
5. W. DAVIS, "Technique for developing design tools from the analysis methods of computational aerodynamics," AIAA Paper 79-1529, 1979 (unpublished).
6. P. GARABEDIAN, *J. Anal. Math.* **30**, 164 (1976).
7. P. GARABEDIAN AND G. MCFADDEN, *AIAA J.* **20**, 289 (1982).
8. A. JAMESON AND D. A. CAUGHEY, "Numerical calculation of the transonic flow past a swept wing," ERDA Research and Development Report COO-3077-136, Courant Inst. Math. Sci., New York University, 1977 (unpublished).
9. E. M. MURMAN AND J. D. COLE, *AIAA J.* **9**, 114 (1971).
10. D. S. ROSS, "Computation of the Transonic Flow about a Swept Wing in the Presence of an Engine Nacelle," DOE/ER/03077-267, Courant Inst. Math. Sci., New York University, 1985 (unpublished).